Computational Analysis of Graphene-Based Periodic Structures via a Three-Dimensional Field-Flux Eigenmode Finite Element Formulation

Vasilis Salonikios, Michalis Nitas, Savvas Raptis, and Traianos V. Yioultsis[*]

Abstract—We present a three-dimensional finite element (FEM) field-flux eigenmode formulation, able to provide accurate modeling of the propagation characteristics of periodic structures featuring graphene. The proposed formulation leads to a linear eigenmode problem, where the effective refractive index is a unknown eigenvalue; the electric field intensity and magnetic flux density are the state variables; and graphene's contribution is efficiently incorporated via a finite conductivity boundary condition. The FEM formulation is spurious-mode free and capable of providing accurate dispersion diagrams and field distributions for arbitrary propagation directions, as opposed to other analytical or numerical approaches, while also efficiently dealing with graphene's dispersive nature. The novelty of the presented approximation is substantiated by computational results for structures incorporating graphene of random periodicity, both within passbands and bandgap frequencies.

1. INTRODUCTION

In the past decade, graphene, i.e., a two-dimensional carbon allotrope, has attracted significant interest due to its infinitesimally small thickness and unique characteristics, such as the ability to support highly confined surface plasmon polariton (SPP) propagation at the far infrared regime [1, 2]. In particular, there has been significant interest for applications utilizing the plasmonic properties of graphene, with the most prevalent examples being THz waveguides and antennas. For instance, there are several applications of graphene in THz detector technology, based on antenna-coupled graphene field-effect transistors [3], photodetectors [4], plasma-wave based detectors [5], plasmonic nanoparticle photodetectors [6], etc. On the other hand, several techniques focus on the experimental characterization of plasmonic effects in graphene, including acoustic or interband plasmons, especially on metal foils [7–12], where properties such as dispersion and damping can be efficiently measured via electron energy loss spectroscopy (EELS) techniques or transmission electron microscopy (TEM) [13].

In many cases, structures in THz applications of this kind very often feature some kind of periodicity on graphene, either in the form of periodically modulated conductivity or in the form of discontinuities in the graphene surface. Configurations like these have shown great potential in tailoring propagation characteristics and improving the excitation techniques of the graphene plasmonic modes [14–22]. Most of these cases that appear in the literature are analyzed using complex analytical techniques that deal with a periodic modulation of the geometric configuration or material properties of graphene. However, the analysis of periodic sharp discontinuities or more complex periodic profiles and arrangements requires a rigorous periodic analysis, which will be able to capture both geometric periodicity and all electromagnetic wave propagation characteristics, including proper calculation of propagation constant,

loss modeling, the presence of bandgaps, the modeling of evanescent modes within them, and the inherent dispersive characteristics of graphene.

In this paper, we propose a general framework and a formulation that deals with all these issues successfully and provides a reliable numerical tool for an accurate approximation of propagation characteristics for graphene-based periodic structures, in terms of their complex propagation constant (eigenvalues) and profiles of the supported eigenmodes (eigenvectors). This is under the assumption of arbitrary wave propagation direction, for graphene structures of arbitrarily shaped periodic inclusions. The analysis is also capable of taking into account graphene's dispersion in a straightforward manner, since the frequency of operation is introduced as an independent variable, and the eigenvalue analysis directly provides the complex propagation constants of various modes, or equivalently, their complex effective refractive indices. The resulting eigenvalue problem is well-conditioned, and its numerical discretization is performed by proper FEM bases, being therefore free of spurious modes.

2. FIELD-FLUX EIGENMODE FORMULATION FOR PERIODIC GRAPHENE STRUCTURES

2.1. The Modified Maxwellian System of Equations

The finite element field-flux formulation is based on the system of Maxwell's equations solved for both the electric field $\mathbf{E}$ and magnetic flux density $\mathbf{B}$, and follows a framework similar to [23]. For the purposes of scaling and alleviation of ill-conditioning in numerical discretization of the Maxwell's system, we scale the magnetic flux density with the vacuum wave velocity as follows:

$$\tilde{\mathbf{B}} = -jc_0\mathbf{B}. \tag{1}$$

Introducing the scaled magnetic flux into Maxwell's equations, we get the scaled system of equations

$$\nabla \times \mathbf{E} = k_0\tilde{\mathbf{B}}, \tag{2}$$

$$\nabla \times \hat{\mu}_r^{-1}\tilde{\mathbf{B}} = k_0\hat{\varepsilon}_r\mathbf{E}, \tag{3}$$

where k_0 is the vacuum wavenumber, and $\hat{\varepsilon}_r$ and $\hat{\mu}_r$ are the relative dielectric permittivity and magnetic permeability tensors.

The symmetry of structures featuring periodic variance along the propagation axis allows us to reduce the computational space to a three-dimensional periodic cell by imposing the Bloch-Floquet periodic boundary condition on the corresponding ports. In addition, we note that graphene's conductivity is a function of frequency, and that the lossy nature of graphene renders the propagation length a very important part of the dispersion analysis. Therefore, for such a problem it is desirable to calculate the wavenumber as a function of a given frequency rather than vice versa. To this end, we assume an arbitrary propagation direction in the form of a known unit vector $\hat{\mathbf{k}}$, and the corresponding wave vector can be expressed as $\mathbf{k} = k_0 n_{\text{eff}}\hat{\mathbf{k}}$, where n_{eff} is the unknown effective refractive index of the wave. Restricting the computational space in a unitary cell of the periodic structure allows us to cast the electric and magnetic field in Bloch form

$$\mathbf{E} = \mathbf{e}e^{-jn_{\text{eff}}k_0\hat{\mathbf{k}}\cdot\bar{\mathbf{r}}}, \tag{4}$$

$$\tilde{\mathbf{B}} = \tilde{\mathbf{b}}e^{-jn_{\text{eff}}k_0\hat{\mathbf{k}}\cdot\bar{\mathbf{r}}}, \tag{5}$$

where $\mathbf{e}$ and $\tilde{\mathbf{b}}$ are the vectorial periodic envelopes of the electric and magnetic fields, which constitute the state variables of the problem. Restating Eqs. (2) and (3) with respect to the Bloch transformation leads to the modified Maxwellian system

$$\nabla \times \mathbf{e} - jn_{\text{eff}}k_0\left(\hat{\mathbf{k}} \times \mathbf{e}\right) = k_0\tilde{\mathbf{b}}, \tag{6}$$

$$\nabla \times \hat{\mu}_r^{-1}\tilde{\mathbf{b}} - jn_{\text{eff}}k_0\left(\hat{\mathbf{k}} \times \hat{\mu}_r^{-1}\tilde{\mathbf{b}}\right) = k_0\hat{\varepsilon}_r\mathbf{e}. \tag{7}$$

This system defines a generalized linear eigenvalue problem in terms of n_{eff}, for which the known operating frequency f is inserted as an independent parameter via $k_0 = 2\pi f/c_0$, along with the proper boundary conditions for the periodic envelopes $\mathbf{e}$ and $\tilde{\mathbf{b}}$.

2.2. Weak Formulation of the Modified Maxwellian System

In order to formulate the eigenvalue problem of the modified Maxwellian system in its variational form, we must first identify the admissible functional spaces of the electric field and magnetic flux density. It is well established that the electric field belongs to the Sobolev space $H(curl, \Omega)$, i.e., the space of measurable functions, with respect to the L^2 norm, with a measureable curl, where Ω denotes the computational space [24]. On the other hand, the admissible function space of the magnetic flux density is determined by examination of the de Rham complex [25]. We only need to observe that the magnetic flux density lies in the range of the curl operator applied to the electric field, and as a result the corresponding functional space of $\mathbf{B}$ is the Sobolev space $H(div, \Omega)$, i.e., the space of measurable, with respect to the L^2 norm, functions with a measureable norm.

The weak formulation of the problem is obtained by applying Galerkin's technique on the modified Maxwellian system. For this purpose, Equation (6) is weighed with testing functions for the magnetic flux density while Eq. (7) is weighed with the testing functions for the electric field

$$\iiint_\Omega \mathbf{b}' \cdot \nabla \times \mathbf{e}\, dv - k_0 \iiint_\Omega \mathbf{b}' \cdot \tilde{\mathbf{b}}\, dv - j n_{\text{eff}} k_0 \iiint_\Omega \mathbf{b}' \cdot \hat{\mathbf{k}} \times \mathbf{e}\, dv = 0, \tag{8}$$

$$\iiint_\Omega (\nabla \times \mathbf{e}') \cdot \hat{\mu}_r^{-1} \tilde{\mathbf{b}}\, dv + \oiint_{d\Omega} \mathbf{e}' \cdot \hat{\mathbf{n}} \times \hat{\mu}_r^{-1} \tilde{\mathbf{b}}\, ds - k_0 \iiint_\Omega \mathbf{e}' \cdot \hat{\varepsilon}_r \mathbf{e}\, dv - j n_{\text{eff}} k_0 \iiint_\Omega \mathbf{e}' \cdot \hat{\mathbf{k}} \times \hat{\mu}_r^{-1} \tilde{\mathbf{b}}\, dv = 0, \tag{9}$$

where $\hat{\mathbf{n}}$ is the normal unit vector pointing outward from the exterior boundary surface. The formulation of the problem is completed by imposing the appropriate boundary conditions. In particular, imposition of impedance boundaries and absorbing boundary conditions (ABCs) are inserted in a straightforward manner via the surface integral, while the enforcement of periodicity is accomplished simply by imposing continuity conditions for the vectorial envelopes of $\mathbf{e}$ and $\tilde{\mathbf{b}}$ at the periodic boundaries.

2.3. Implementation of Graphene

Consistent treatment of graphene is an essential feature of the proposed formulation, due to its extremely small thickness. Since the thickness of a graphene monolayer is clearly in the sub-nanometer range, it is not recommended to model it as a bulk material with finite thickness. Such a model would necessitate the use of extremely fine meshing within the graphene's width and also lead to extremely flat or "sliver" finite elements, which in turn can be detrimental to FEM matrix scaling and conditioning.

Instead, we model graphene as an ideal two-dimensional surface of infinitesimal thickness. This allows interpreting its contribution to the overall electromagnetic system as a surface current density, or a sheet of finite conductivity that can be readily inserted in the formulation. First, we consider the graphene sheet as a two-sided exterior boundary S, which lies outside the computational domain. This is done by considering an exterior boundary surface $S^+ \cup S^-$ which closely surrounds graphene from both sides (Figure 1). The upper part S^+ of the surface is at an infinitesimal distance above graphene, whereas the lower part S^- is likewise below it. We can now apply the surface current interface condition
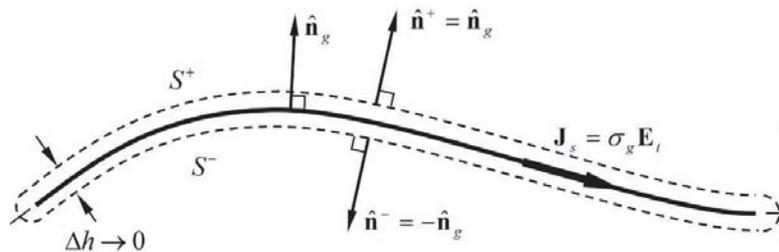

Figure 1. Two-dimensional cut of a graphene sheet of infinitesimal thickness, surrounded by a shrinking closed surface. The closed surface is considered an outer boundary of the computational domain, i.e., all inner volume, including graphene, is excluded from the computational domain.

on the sheet's surface

$$\hat{\mathbf{n}}_g \times \hat{\mu}_r^{-1}\mathbf{B}^+\big|_S - \hat{\mathbf{n}}_g \times \hat{\mu}_r^{-1}\mathbf{B}^-\big|_S = \mathbf{J}_s = \sigma_g\mathbf{E}_t, \tag{10}$$

where $\hat{\mathbf{n}}_g$ is the unit vector normal to graphene's surface; σ_g is the graphene's conductivity (in S, since surface current is in A/m); and $\mathbf{E}_t$ is the tangential electric field component along graphene. Using transformations in Eqs. (4) and (5), we get the modified condition

$$\hat{\mathbf{n}}_g \times \hat{\mu}_r^{-1}\tilde{\mathbf{b}}^+\Big|_S - \hat{\mathbf{n}}_g \times \hat{\mu}_r^{-1}\tilde{\mathbf{b}}^-\Big|_S = -j\eta_0\sigma_g\mathbf{e}_t, \tag{11}$$

where η_0 is the free space intrinsic impedance. We now consider the part of the surface integral term in Eq. (9) related to the graphene sheet, which can be written in two parts, considering the upper and lower parts of the surrounding surface $S^+ \cup S^-$. Since the outward pointing unit vectors normal to S^+ and S^- are $-\hat{\mathbf{n}}_g$ and $\hat{\mathbf{n}}_g$, respectively, the graphene-related surface integral term of Eq. (9) takes the form

$$I_g = \iint\limits_{S^+} \mathbf{e}' \cdot \hat{\mathbf{n}} \times \hat{\mu}_r^{-1}\tilde{\mathbf{b}}^+ ds + \iint\limits_{S^-} \mathbf{e}' \cdot \hat{\mathbf{n}} \times \hat{\mu}_r^{-1}\tilde{\mathbf{b}}^- ds = -\iint\limits_{S} \mathbf{e}' \cdot \left(\hat{\mathbf{n}}_g \times \hat{\mu}_r^{-1}\tilde{\mathbf{b}}^+ - \hat{\mathbf{n}}_g \times \hat{\mu}_r^{-1}\tilde{\mathbf{b}}^-\right) ds, \tag{12}$$

where S^+ and S^- are assumed to shrink to the graphene surface S, while retaining the discontinuity of tangential magnetic fields. Finally, considering the interface condition in Eq. (11), the surface integral term is written in the simple form

$$I_g = j\eta_0 \iint\limits_{S} \mathbf{e}'_t \cdot \sigma_g\mathbf{e}_t ds, \tag{13}$$

which resembles a standard form of an FEM mass matrix, this time in surface form. It has to be noted that discretization of this term is straightforward and is done on the facets of the interface, without the need to consider graphene as a bulk material. Therefore, we avoid the associated volumetric representation and discretization, which would be meaningless for a single atomic layer material, but also adverse from the point of view of computational efficiency and consistency.

2.4. The Final Eigenvalue Problem

The last step in configuring the eigenvalue problem is to approximate the weak formulation of Eqs. (8) and (9) with a finite dimensional problem by discretizing the electric field and magnetic flux density using finite element spaces. For this purpose, the electric field is expanded in the finite dimensional subset of the $H(curl, \Omega)$ space, consisting of tangentially continuous edge-type basis functions, while the magnetic flux density is expanded in the finite dimensional subset of $H(div, \Omega)$, consisting of normally continuous facet-type basis functions [26]. The final system represents a mixed finite element eigenvalue problem and has the matrix form

$$\begin{bmatrix} -k_0\mathbf{T}^{EE} + j\eta\mathbf{T}_s^{EE} & \mathbf{Q}^{EB} \\ \mathbf{Q}^{BE} & -k_0\mathbf{T}^{BB} \end{bmatrix} \begin{bmatrix} \mathbf{E} \\ \mathbf{B} \end{bmatrix} = jn_{\text{eff}} \begin{bmatrix} 0 & k_0\mathbf{P}^{EB} \\ k_0\mathbf{P}^{BE} & 0 \end{bmatrix} \begin{bmatrix} \mathbf{E} \\ \mathbf{B} \end{bmatrix}. \tag{14}$$

The submatrices of Eq. (14) are the assembled matrices corresponding to each one of the terms appearing in Eqs. (8) and (9), with the surface integral term $\mathbf{T}_s^{EE}$ calculated as a discretization of Eq. (13).

The pencil matrix of Eq. (14) defines a linear eigenvalue problem that does not require the application of any computationally costly linearization technique and is spurious-mode free, owing to the use of appropriate element bases and the avoidance of the curl-curl operators. A further advantage is that both computed fields are of the same order of approximation, which is also important to avoid any differentiation in applying post-processing homogenization techniques. Moreover, the choice of n_{eff} as the eigenvalue improves the overall conditioning of the problem, by properly balancing the norms of the two matrices comprising the pencil matrix and also simplifies the process by reducing the spectral range. It is noted that the proposed formulation was implemented both as an in-house code and in the Weak Form of COMSOL Multiphysics®, resulting in identical results when being solved for identical meshes and degrees of freedom. Therefore, the proposed technique can also be easily accommodated in a commercial EM analysis software that facilitates the solution of user defined boundary value problems.

Finally, it should be emphasized that if the eigenvalue problem were to be treated the other way around, with the classical β-ω procedure usually followed in the analysis of photonic crystals, the propagation constant β should be actually the variable to be *a priori* specified. It would, thus, span the entire irreducible Brillouin zone $0 \le \beta \le \pi/d$, where d is the spatial period, and the frequency ω would be the unknown eigenvalue. The grave disadvantage of this approach is that modeling of losses cannot be directly incorporated, with the additional inherent inability to consider graphene's conductivity as a function of frequency. In particular, the frequency term at Kubo's formula lies at the denominator of the fraction [27], which renders an FEM formulation of this kind practically inapplicable. Moreover, such an analysis provides no information inside the bandgap. The proposed FEM formulation alleviates all these issues, and in addition, the propagation length $L_{\mathrm{SPP}} = 2\pi/a$, which is an essential parameter to quantify losses of surface plasmons waveguiding structures, is directly evaluated through the readily available imaginary part of the extracted eigenvalues, i.e., $a = \mathrm{Re}\{\gamma\} = \mathrm{Re}\{jk_0 n_{\mathrm{eff}}\} = -jk_0\mathrm{Im}\{n_{\mathrm{eff}}\}$. Therefore, the overall analysis provides a proper computational tool for the extraction of the dispersion behavior of periodic structures that include graphene.

3. COMPUTATIONAL RESULTS

3.1. Free-Standing Graphene Micro-Ribbon

To validate the proposed formulation, we have examined the well-documented case of a free-standing graphene ribbon of $5\,\mu\mathrm{m}$ width. Graphene's conductivity was evaluated via the Kubo formula [1] at room temperature $T = 300\,\mathrm{K}$ with the energy independent scattering rate Γ equal to $0.1\,\mathrm{meV}$ and a chemical potential of $0.2\,\mathrm{eV}$. The dispersion diagram of the first three modes supported by the graphene ribbon is depicted in Figure 2(a), whereas the corresponding propagation length $L_{\mathrm{SPP}} = 2\pi/a$ is shown in Figure 2(b). Furthermore, the analytical results for the dispersion equation and the propagation length of the infinite graphene layer are also drawn in these figures, with $n_{\mathrm{eff}} = \sqrt{1 - 4/(n_0\sigma_g)^2}$ as proven in [28]. Examination of the dispersion of these modes reveals the highly confined nature of the graphene SPPs, as the higher refractive index is related to the confinement of moving charges. The distribution of the axial and transverse components (magnitude) of the electric field on a plane transverse to the propagation axis for the all modes are displayed in Figure 3. In all three cases, the concentration of the electric field on graphene's surface is evident. Finally, the dispersion diagram and the distribution of the electric field are in full agreement with the existing literature [1, 14, 27] and thus validate the accuracy of the proposed formulation.

3.2. Periodic Arrangement of Graphene Micro-Strips

The capabilities of the 3D field-flux eigenmode formulation were also tested against the more complex problem of a periodic arrangement of free-standing graphene micro-strips of $5\,\mu\mathrm{m}$ width, which can also be viewed as a graphene ribbon with periodic separation gaps along the axis of propagation. As in the case of the free-standing graphene micro-ribbon, graphene's conductivity was evaluated via the Kubo formula, in order to use the results of the first validation test as a reference. The computational domain of the problem is the unit cell of the structure in Figure 4, whereas the geometrical parameters of the structure were selected as $g = 0.5\,\mu\mathrm{m}$ and $R = 10\,\mu\mathrm{m}$.

Based on these aspects, the search for the eigenvalues of this problem is performed for propagation constants inside the irreducible Brillouin zone, and the extracted dispersion diagram and the corresponding propagation lengths with respect to frequency are shown in Figure 5. A minor issue that needs to be addressed is the presence of complex "box" modes, i.e., plane waves reflected from the exterior boundary conditions and perturbed by the presence of graphene, which are nevertheless strongly evanescent and can be easily removed. In addition, the electric field distributions of the modes under examination for the transverse and normal plane of the structure are illustrated in Figure 6 (first mode) and in Figure 7 (second mode). The numbering of the modes in the periodic structure is equivalent to the numbering of the graphene ribbon modes, linking them by the distribution of the electric field at the plane transverse to propagation direction.

Examination of the dispersion diagram reveals that the modulation of the graphene micro-ribbon introduces spectral areas of fast-wave propagation. This becomes more prominent for the higher end
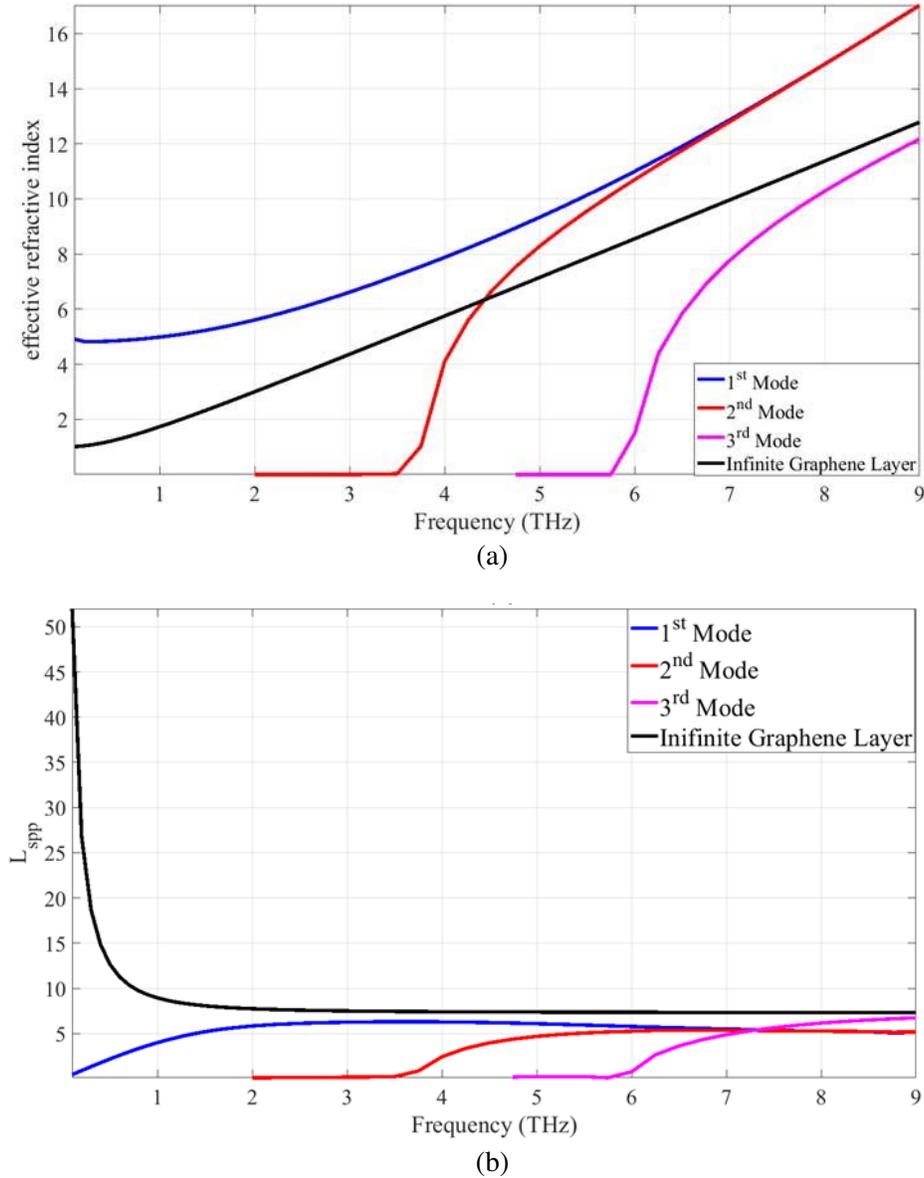
Figure 2. (a) Dispersion curves in terms of the effective refractive index of the first three modes of a 5 μm graphene ribbon compared to the infinite layer. (b) Normalized propagation length of the first three modes shown together with the infinite layer case.

of the spectrum under consideration and indicates that at those frequencies a configuration of this form could operate as a diffraction grating or a leaky-wave antenna [29]. The presence of two bandgap regions is also visible in the frequency ranges of 3 THz to 3.4 THz and 4 THz to 4.4 THz. These bandgaps owe their existence to the periodic configuration of the structure and can also be distinguished by the rapid decline of the propagation length. The introduction of gaps further differentiates the two modes under consideration. In the case of the graphene ribbon, these two modes converge to the dispersion curve of the infinite graphene layer. However, this behaviour is not evident in the case of the periodic arrangement of graphene micro-strips as the corresponding dispersion curves in the irreducible Brillouin zone are almost parallel to each other. It also appears that the second mode of the periodic graphene structure retains the same cut-off frequency as its graphene ribbon counterpart, and as a result, the single mode region remains unchanged.

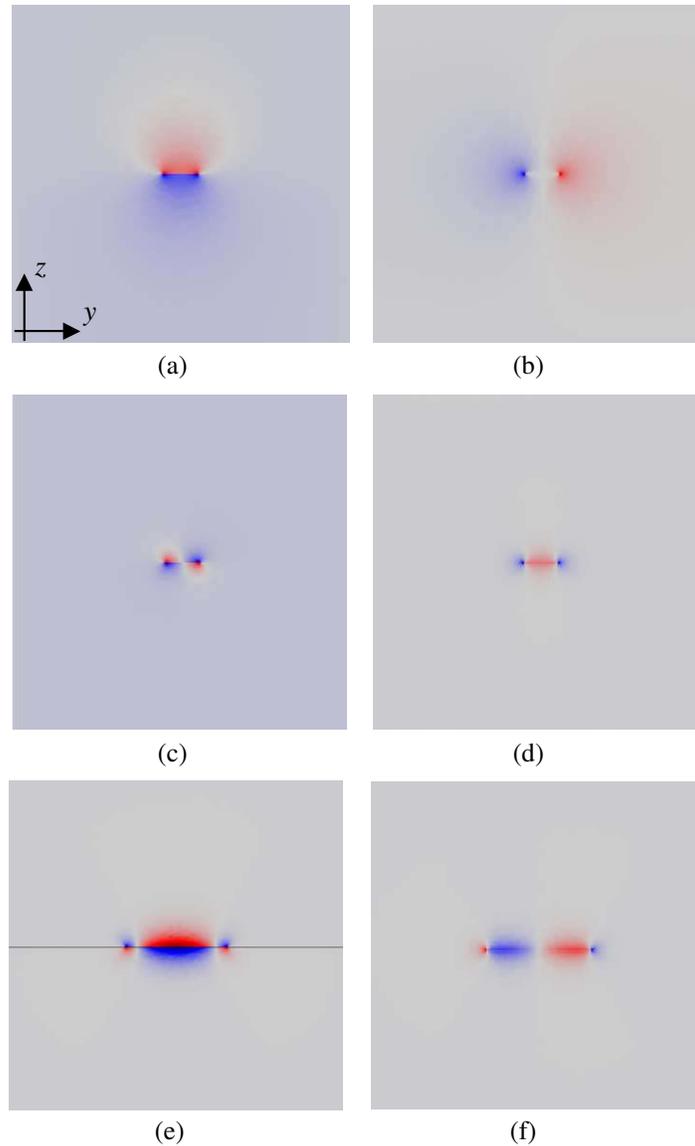The inspection of the field distributions of the two modes inside the passbands affirms the

Figure 3. Transverse electric field distribution of a 5 μm wide graphene micro-ribbon SPP: (a) axial and (b) transverse components of the first mode (1 THz), (c) axial and (d) transverse components of the second mode (4.5 THz) and (e) axial and (f) transverse components of the third mode (9 THz).
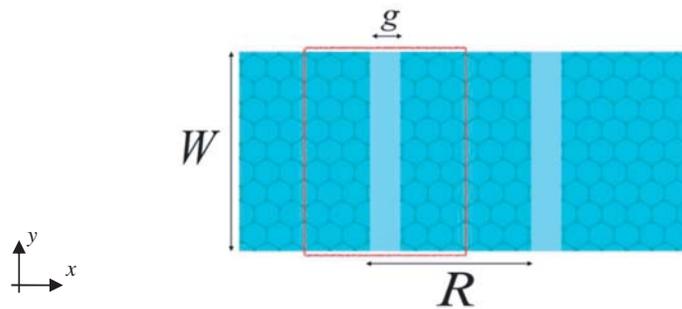

Figure 4. Periodic arrangement of graphene micro-strips separated by a gap of width, g. The spatial period of the structure is R and a top-view of the 3D unit cell under examination appears enclosed by the red frame.
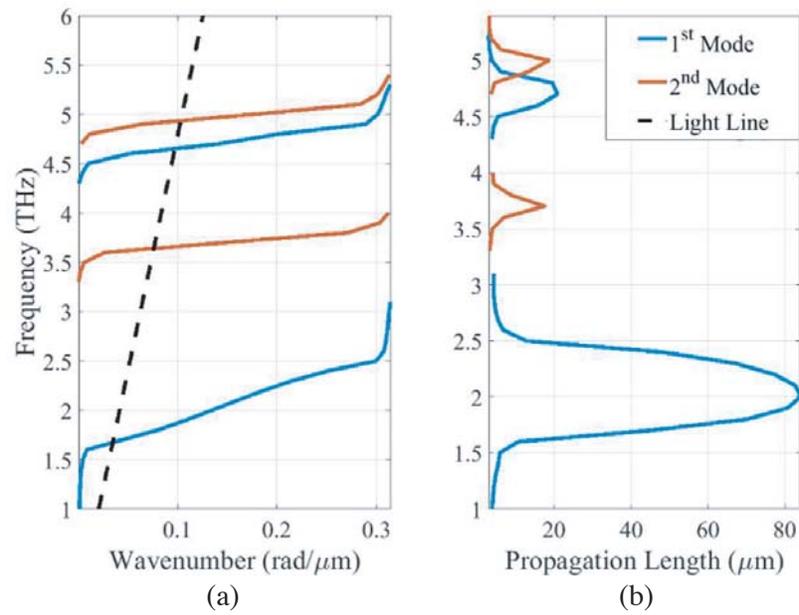
(a)

(b)

Figure 5. (a) Dispersion diagram and (b) propagation length of a periodic arrangement of graphene micro-strips with respect to frequency.

(a)   (b)

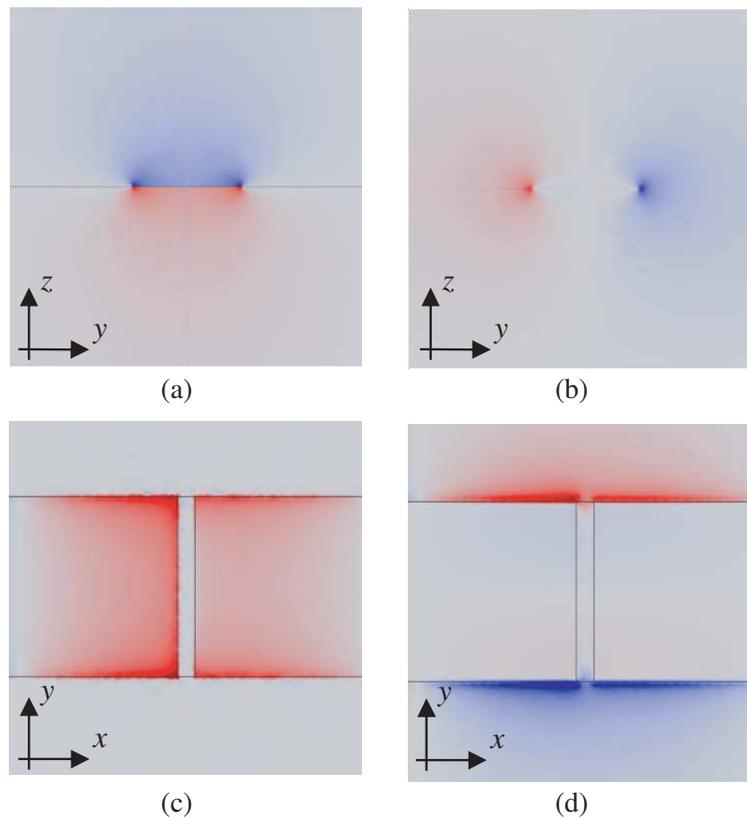(c)   (d)

Figure 6. Electric field distributions of the first mode of the periodic arrangement of graphene micro-strips at 2.5 THz: (a) axial and (b) transverse components on the plane transverse to propagation, (c) normal and (d) tangential component directly above the graphene surface.
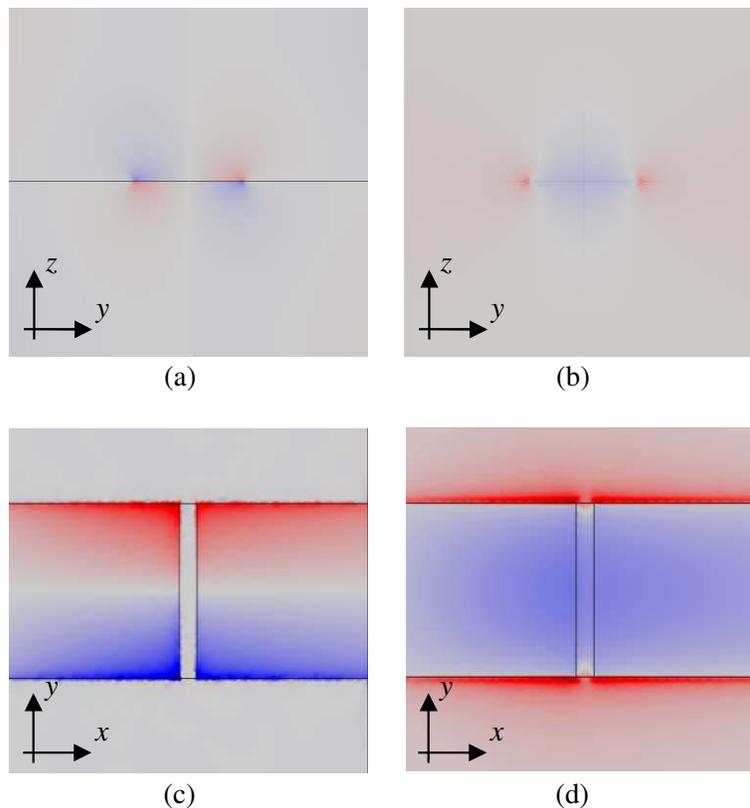
Figure 7. Electric field distributions of the second mode of the periodic arrangement of graphene micro-strips at 3.5 THz: (a) axial and (b) transverse components on the plane transverse to propagation, (c) normal and (d) tangential component directly above the graphene surface.

confinement of the electric field to the graphene surface. Both modes of the periodic structure retain the tangential profile of the corresponding graphene ribbon modes, while the tangential components of the electric field appear less affected from the introduction of the gaps, than the normal ones.

4. CONCLUSIONS

We have presented a mixed finite element eigenmode solver for periodic structures featuring graphene, based on a modified Maxwellian formulation that solves the electromagnetic problem in terms of both the electric field intensity and magnetic flux density simultaneously. Graphene's contribution is properly and efficiently modeled as a finite conductivity boundary, i.e., an infinitesimally thin sheet, and the formulation is capable of acquiring complex propagation constants and field distributions of complex configurations featuring graphene, both within passbands and bandgaps. The proposed formulation is validated by results simulating free standing graphene strips and periodically arranged graphene microstrips and can serve as an efficient tool to study wave propagation in periodic graphene configurations, with a straightforward generalization to anisotropic graphene and also the potential to deal with nonlinear graphene problems [30].

ACKNOWLEDGMENT

REFERENCES

1. Nikitin, A. Y., F. Guinea, F. J. García-Vidal, and L. Martín-Moreno, "Edge and waveguide terahertz surface plasmon modes in graphene microribbons," *Phys. Rev. B*, Vol. 84, 161407, 2011.

2. Politano, A. and G. Chiarello, "Plasmon modes in graphene: Status and prospect," *Nanoscale*, Vol. 6, 10927–10940, 2014.

3. Vicarelli, L., M. S. Vitiello, D. Coquillat, A. Lombardo, A. C. Ferrari, W. Knap, M. Polini, V. Pellegrini, and A. Tredicucci, "Graphene field-effect transistors as room-temperature terahertz detectors," *Nat. Mater.*, Vol. 11, 865–871, 2012.

4. Tomadin, A., A. Tredicucci, V. Pellegrini, M. S. Vitiello, and M. Polini, "Photocurrent-based detection of terahertz radiation in graphene," *Appl. Phys. Lett.*, Vol. 103, 211120, 2013.

5. Spirito, D., D. Coquillat, S. L. De Bonis, A. Lombardo, M. Bruna, A. C. Ferrari, V. Pellegrini, A. Tredicucci, W. Knap, and M. S. Vitiello, "High performance bilayer-graphene terahertz detectors," *Appl. Phys. Lett.*, Vol. 104, 061111, 2014.

6. Koppens, F. H. L., T. Mueller, P. Avouris, A. C. Ferrari, M. S. Vitiello, and M. Polini, "Photodetectors based on graphene, other two-dimensional materials and hybrid systems," *Nat. Nanotechnol.*, Vol. 9, 780–793, 2014.

7. Politano, A., H. K. Yu, D. Farías, and G. Chiarello, "Multiple acoustic surface plasmons in graphene/Cu(111) contacts," *Phys. Rev. B*, Vol. 97, 035414, 2018.

8. Politano, A., I. Radović, D. Borka, Z. L. Mišković, H. K. Yude, D. Farías, and G. Chiarello, "Dispersion and damping of the interband π plasmon in graphene grown on Cu(111) foils," *Carbon*, Vol. 114, 70–76, 2017.

9. Politano, A., I. Radović, D. Borkab, Z. L. Mišković, and G. Chiarello, "Interband plasmons in supported graphene on metal substrates: Theory and experiments," *Carbon*, Vol. 96, 91–97, 2016.

10. Politano, A., A. R. Marino, V. Formoso, D. Farías, R. Miranda, and G. Chiarello, "Quadratic dispersion and damping processes of π plasmon in monolayer graphene on Pt(111)," *Plasmonics*, Vol. 7, 369–376, 2012.

11. Politano, A., A. R. Marino, V. Formoso, D. Farías, R. Miranda, and G. Chiarello, "Evidence for acoustic-like plasmons on epitaxial graphene on Pt(111)," *Phys. Rev. B*, Vol. 84, 033401, 2011.

12. Cupolillo, A., A. Politano, N. Ligato, D. M. Cid Perez, G. Chiarello, and L. S. Caputi, "Substrate-dependent plasmonic properties of supported graphene," *Surf. Sci.*, Vol. 634, 76, 2015.

13. Politano, A., G. Chiarello, and C. Spinella, "Plasmon spectroscopy of graphene and other two-dimensional materials with transmission electron microscopy," *Mater. Sci. Semicond. Process.*, Vol. 65, 88–99, 2017.

14. Ben Rhouma, M., M. Oueslati, and B. Guizal, "Surface plasmons on a doped graphene sheet with periodically modulated conductivity," *Superlattices and Microstructures*, Vol. 96, 212–219, 2016.

15. Nikitin, A. Yu., F. Guinea, F. J. Garcia-Vidal, and L. Martin-Moreno, "Surface plasmon enhanced absorption and suppressed transmission in periodic arrays of graphene ribbons," *Phys. Rev. B*, Vol. 84, 161407, 2011.

16. Bludov, Y. V., N. M. R. Peres, and M. I. Vasilevskiy, "Graphene-based polaritonic crystal," *Phys. Rev. B*, Vol. 85, 081405, 2012.

17. Ferreira, A. and N. M. R. Peres, "Complete light absorption in graphene-metamaterial corrugated structures," *Phys. Rev. B*, Vol. 86, 205401, 2012.

18. Madani, A., S. Zhong, H. Tajalli, S. R. Entezar, A. Namdar, and Y. Ma, "Tunable metamaterials made of graphene-liquid crystal multilayers," *Progress In Electromagnetics Research*, Vol. 143, 545–558, 2013.

19. Freitag, M., et al., "Photocurrent in graphene harnessed by tunable intrinsic plasmons," *Nature Comm.*, Vol. 4, 1951, 2013.

20. Gómez-Díaz, J. S., M. Esquius-Morote, and J. Perruisseau-Carrier, "Plane wave excitation-detection of non-resonant plasmons along finite-width graphene strips," *Optics Express*, Vol. 21, 24856–24872, 2013.

21. Malhat, H. A., S. H. Zainud-Deen, and S. M. Gaber, "Graphene based transmitarray for terahertz applications," *Progress In Electromagnetics Research M*, Vol. 36, 185–191, 2014.

22. Juneghani, F. A., A. Z. Nezhad, and R. Safian, "Analysis of diffraction graphene gratings using the C-method and design of a terahertz polarizer," *Progress In Electromagnetics Research M*, Vol. 65, 175–186, 2018.

23. Nitas, M., C. S. Antonopoulos, and T. V. Yioultsis, "EB eigenmode formulation for the analysis of lossy and evanescent modes in periodic structures and metamaterials," *IEEE Trans. Magnetics*, Vol. 53, 2017.

24. Monk, P., *Finite Element Methods for Maxwell's Equations*, Oxford University Press, 2003.

25. Boffi, D., F. Brezzi, and M. Fortin, *Mixed Finite Element Methods and Applications*, Springer, Heidelberg, 2013.

26. Zhu, Y. and A. C. Cangellaris (eds.), *Multigrid Finite Element Methods for Electromagnetic Field Modeling*, John Wiley & Sons, 2006.

27. Salonikios, V., S. Amanatiadis, N. Kantartzis, and T. V. Yioultsis, "Modal analysis of graphene microtubes utilizing a two-dimensional vectorial finite element method," *Applied Physics A*, Vol. 122, 351, 2016.

28. Hanson, G. W., "Dyadic Green's functions and guided surface waves for a surface conductivity model of graphene," *J. Appl. Phys.*, Vol. 103, 064302, 2008.

29. Gonçalves, P. A. D., E. J. C. Dias, Y. V. Bludov, and N. M. R. Peres, "Modeling the excitation of graphene plasmons in periodic grids of graphene ribbons: An analytical approach," *Phys. Rev. B*, Vol. 94, 195421, 2016.

30. Politano, A. and G. Chiarello, "Emergence of a nonlinear plasmon in the electronic response of doped graphene," *Carbon*, Vol. 71, 176–80, 2014.